Pergamon

Int. J. Heat Mass Transfer. Vol. 38, No. 7, pp. 1201–1216, 1995

0017-9310/95 $9.50+0.00

0017-9310(94)00244-4

Experimental and numerical study of quenching complex-shaped metallic alloys with multiple, overlapping sprays

DAVID D. HALL and ISSAM MUDAWAR†

Boiling and Two-Phase Flow Laboratory, School of Mechanical Engineering, Purdue University, West Lafayette, IN 47907, U.S.A.

(*Received* 20 *May* 1994 *and in final form* 22 *July* 1994)

Abstract—The present study constitutes a crucial step towards the development of a CAD based intelligent spray quenching system capable of optimizing the mechanical properties (strength, hardness) of age-hardenable aluminum alloys. The quenching of an L-shaped aluminum alloy with multiple, partially overlapping spray nozzles was successfully modeled using the finite element method. Spray heat transfer correlations, which relate the local heat transfer rate in each of the boiling regimes experienced by the surface to the local values of the spray hydrodynamic parameters (volumetric spray flux, mean drop diameter, mean drop velocity), were used as boundary conditions. The spatial distributions of the spray hydrodynamic parameters were modeled and incorporated into the finite element program. Axial non-uniformity in the heat transfer coefficient along the surfaces of long extrusions, which can lead to unwanted residual stresses, was eliminated by developing a method for optimizing the distance between adjacent nozzles. The numerical results were experimentally verified in a simulated industrial environment. This study is the first successful attempt at systematically predicting the temperature response of a quenched part from knowledge of only the part geometry and spray nozzle configuration. Integration of the finite element program with an optimization routine will yield a system capable of selecting the appropriate spray nozzle configuration for a new part prior to production; thus, achieving superior part quality without conducting costly experimental tests.

INTRODUCTION

Increased competitiveness in the materials processing industry has demanded the development of more efficient production methods to satisfy increasingly tougher specifications while significantly reducing cost. The final mechanical and metallurgical properties of age-hardenable aluminum alloy extrusions are contingent upon the rate at which the part is cooled (quenched) after the high temperature forming process. If the exterior of a part having a cross-section with large variations in thickness is cooled as quickly as possible, large spatial temperature gradients develop which lead to high residual stresses and warping. Conversely, if a part is cooled too slowly, uniform cooling may exist, but the desired strength or hardness cannot be obtained in the subsequent age-hardening heat treatment. Thus, an intelligent spray quenching system is proposed which will determine how to cool a part as quickly and uniformly as possible such that the resulting mechanical properties are optimized with minimal cost.

The spray quenching process consists of directing high pressure liquid sprays onto areas of the part where higher cooling rates are required. The operator selects an initial nozzle configuration and operating pressure, based on experience and the visual appearance of the part, such that uniform cooling is presumed. This trial and error operation frequently leads to high residual stresses, nonuniform properties, low corrosion resistance, warping, soft spots, or cracking, all of which may lead to low strength and premature part failure. The operator subsequently modifies the nozzle configuration until post-heat treatment tests reveal that acceptable mechanical and metallurgical properties were obtained. Only after this testing phase is completed can the continuous production of the part be initiated.

The present study is part of an ongoing research project at the Purdue University Boiling and Two-Phase Flow Laboratory whose primary goal is the development of the CAD based intelligent spray quenching system proposed by Deiters and Mudawar [1] and illustrated in Fig. 1(a). The operator inputs the composition and geometry of the extrusion or forging into the CAD system and, upon consulting its extensive data bases, the CAD system determines the nozzle configuration (type, placement, and pressure) required to obtain acceptable mechanical properties in the heat treated product, thus eliminating the costly trial and error procedure utilized today.

Heat transfer aspects of the heat treatment process

The quenching process is usually initiated at very high temperatures well above the saturation temperature of the liquid coolant. As the surface tem-

† Author to whom correspondence should be addressed.

NOMENCLATURE

c_p	specific heat at constant pressure
d_{32}	Sauter mean diameter (SMD)
h	convection heat transfer coefficient
h_{fg}	latent heat of vaporization
k	thermal conductivity
Nu_{32}	Nusselt number, hd_{32}/k_f
Pr	Prandtl number
q''	heat flux
Q''	volumetric spray flux
$\bar{Q}''$	mean volumetric spray flux along the major axis of the spray field
Re_{32}	Reynolds number, $\rho_f Q'' d_{32}/\mu_f$
t	time
T	temperature
ΔT	$T_s - T_f$
ΔT_{sub}	liquid subcooling, $T_{sat} - T_f$
U_m	mean drop velocity
x	coordinate along spray major axis
y	coordinate along spray minor axis
z	coordinate along the spray centerline.

Greek symbols

μ	dynamic viscosity
ρ	density
σ	surface tension; standard deviation.

Subscripts

CHF	critical heat flux
DFB	departure from film boiling
f	saturated liquid
g	saturated vapor
MIN	minimum heat flux
OSP	onset of single-phase cooling
s	surface condition
sat	saturated condition.

perature decreases, different boiling regimes will be observed with each having distinct heat transfer characteristics. Figure 1(b) shows a typical boiling curve for a hot surface submerged in a liquid bath and the corresponding boiling regimes. The film boiling regime is characterized by an insulating vapor blanket on the surface which prevents the liquid from making direct contact with the surface and results in slow cooling. Once the temperature decreases below the point of minimum heat flux, the vapor blanket begins to collapse and partial wetting of the surface ensues. This transition boiling regime is marked by a significant increase in the surface heat flux due to local areas of intense boiling, thus causing a rapid decrease in surface temperature. The maximum heat flux occurs at the point of critical heat flux (CHF) where the vapor layer begins to vanish causing the cooling rate to become a maximum. In the nucleate boiling regime, the entire surface experiences liquid contact and vigorous bubble production is observed, thus, keeping cooling rates fairly high. Boiling completely subsides in the single-phase cooling regime and the relatively low heat transfer rate is due to natural convection.

Of more relevance to the quenching process is the corresponding temperature–time curve (cooling curve, quench curve) of the surface experiencing boiling, which is shown in Fig. 1(c). While the part geometry and nozzle configuration will alter the cooling rates observed on the surface and within the quenched part, the general shape of the cooling curve will remain unchanged. The most notable feature of Fig. 1(c) is the sharp drop in temperature immediately following the point of minimum heat flux. By predicting and, subsequently, controlling the occurrence of the point of minimum heat flux, it may be possible to delay or advance the onset of the high cooling rates associated with the transition and nucleate boiling regimes such that the mechanical and metallurgical properties are optimized throughout the quenched part.

Spray quenching heat transfer correlations

A series of studies performed at the Purdue University Boiling and Two-Phase Flow Laboratory culminated in the spray quenching heat transfer correlations listed in Table 1. Mudawar and Valentine [2] conducted a comprehensive literature review and concluded that sprays can be characterized in terms of the distribution of spray hydrodynamic parameters (volumetric spray flux, mean drop diameter, and mean drop velocity) just prior to impingement upon the surface. They developed heat transfer correlations universal to all spray types (full cone, hollow cone and flat sprays) for transition boiling, nucleate boiling, and single-phase cooling regimes based on surface temperature and the local spray hydrodynamic parameters. Mudawar and Deiters [3, 4] later concluded these correlations, which were developed from measurements at the geometric center of the sprays, were valid at other locations within the spray field when the spray hydrodynamic parameters are determined for these locations.

Klinzing *et al.* [5] completed the research initiated by Mudawar and Valentine [2] by developing correlations for the film boiling regime and modifying the correlation for the transition boiling regime. Klinzing *et al.* also identified a film wetting regime not shown in Figs. 1(b) and 1(c), characterized by intermittent wetting and reformation of the vapor blanket, which occurs between the point of departure from film boiling and the point of minimum heat flux. Four different full cone spray nozzles and one flat spray nozzle were operated at various pressures and nozzle-to-surface distances to obtain a wide range of spray hydrodynamic parameters. Klinzing *et al.* also identi-

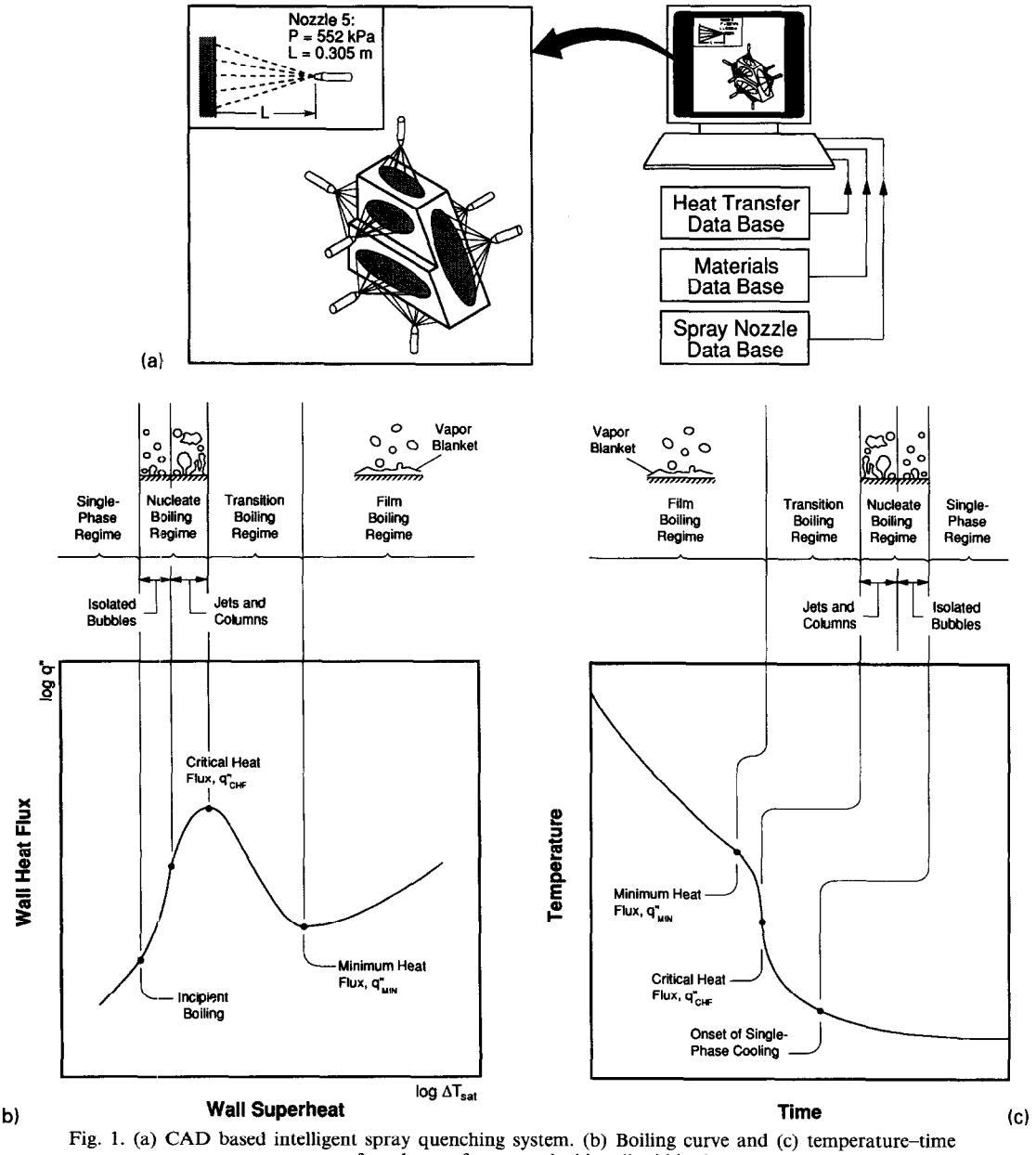

Fig. 1. (a) CAD based intelligent spray quenching system. (b) Boiling curve and (c) temperature–time curve for a hot surface quenched in a liquid bath.

fied two distinct spray cooling regimes based on volumetric spray flux for the boiling regimes they investigated. These spray cooling regimes have been previously identified for the film boiling regime [6] and labeled as dilute sprays, which are characterized by negligible droplet interactions during impaction on the surface, and dense sprays, which are characterized by significant droplet interactions that alter the heat transfer dependence on the spray hydrodynamic parameters. The high spray flux correlations (not shown in Table 1) are applicable to sprays having larger drop diameters and velocities than those used in the present study.

The aforementioned heat transfer correlations completely describe all of the boiling regimes experienced by an aluminum part undergoing a spray quenching operation and may be used as boundary conditions for a numerical analysis which models the spray quenching of an alloy with several nozzles. A method for incorporating these correlations into boundary conditions for parts impacted by multiple overlapping sprays will be introduced later in this paper.

Literature review

Mudawar and Valentine [2] demonstrated that heat transfer to water sprays depends upon the local values of the spray hydrodynamic parameters. Deiters and Mudawar [3] determined that the volumetric spray flux varies considerably throughout the spray field. However, Kim *et al.* [7] and Wang *et al.* [8] assumed

Table 1. Spray quenching heat transfer correlations

Quenching (boiling) regime [ref.]	Correlation
Film boiling regime [5]	$q'' = 6.325\times10^{1}\,\Delta T^{1.691}\,Q''^{0.264}\,d_{32}^{-0.062}$
Point of departure from film boiling [5]	$q''_{DFB} = 6.100\times10^{6}\,Q''^{0.588}\,U_m^{0.244}$
	$\Delta T_{DFB} = 2.808\times10^{2}\,Q''^{0.087}\,U_m^{0.110}\,d_{32}^{-0.035}$
Film-wetting regime [5]	$q'' = q''_{MIN} + (q''_{DFB} - q''_{MIN})\left(\frac{\Delta T - \Delta T_{MIN}}{\Delta T_{DFB} - \Delta T_{MIN}}\right)^2$
Point of minimum heat flux [5]	$q''_{MIN} = 3.324\times10^{6} Q''^{0.544}\,U_m^{0.324}$
	$\Delta T_{MIN} = 2.049\times10^{2} Q''^{0.066}\,U_m^{0.138}\,d_{32}^{-0.035}$
Transition boiling regime [5]	$q'' = q''_{CHF} - \frac{q''_{CHF} - q''_{MIN}}{(\Delta T_{CHF} - \Delta T_{MIN})^3}[\Delta T_{CHF}^3 - 3\Delta T_{CHF}^2\Delta T_{MIN} + 6\Delta T_{CHF}\Delta T_{MIN}\Delta T - 3(\Delta T_{CHF} + \Delta T_{MIN})\Delta T^2 + 2\Delta T^3]$
Point of critical heat flux [2]	$\frac{q''_{CHF}}{\rho_g h_{fg} Q''} = 122.4\left[1 + 0.0118\left(\frac{\rho_g}{\rho_f}\right)^{1/4}\left(\frac{\rho_f c_{p,f}\Delta T_{sub}}{\rho_g h_{fg}}\right)\right]\left(\frac{\sigma}{\rho_f Q''^2 d_{32}}\right)^{0.198}$
	$\Delta T_{CHF} = 18.0\left[(\rho_g h_{fg} Q'')\left(\frac{\sigma}{\rho_f Q''^2 d_{32}}\right)^{0.198}\right]^{1/5.55}$
Nucleate boiling regime [2]	$q'' = 1.87\times10^{-5}(\Delta T)^{5.55}$
Onset of single-phase cooling [2]	$\Delta T_{OSP} = 13.43\,Re_{32}^{0.167}\,Pr_f^{0.123}\left(\frac{k_f}{d_{32}}\right)^{0.220}$
Single-phase regime [2]	$Nu_{32} = 2.512\,Re_{32}^{0.76}\,Pr_f^{0.56}$

Units of the parameters: q''(W m^{-2}), $\Delta T = T_s - T_f$ (°C), Q'' (m^3 s^{-1} m^{-2}), U_m (m s^{-1}), d_{32} (m), h (W m^{-2} K^{-1}), ρ_f (kg m^{-3}), ρ_g (kg m^{-3}), h_{fg} (J kg^{-1}), $c_{p,f}$ (J kg^{-1} K^{-1}), k_f (W m^{-1} K^{-1}), μ_f (N·s m^{-2}), σ (N m^{-1}).

Dimensionless parameters: $Nu_{32} = h\,d_{32}/k_f$, $Pr_f = c_{p,f}\,\mu_f/k_f$, $Re_{32} = \rho_f Q''\,d_{32}/\mu_f$.

Range of validity of the correlations: $T_f = 23$°C, $Q'' = 0.58\times10^{-3} - 9.96\times10^{-3}$ m^3 s^{-1} m^{-2}, $U_m = 10.1$–29.9 m s^{-1}, $d_{32} = 0.137\times10^{-3}$–$1.35\times10^{-3}$ m.

Properties: The fluid properties used in the correlations for the point of incipient boiling and the single-phase regime are evaluated at the film temperature, $T_{film} = 0.5\,(T_s + T_f)$. The fluid properties used in the CHF correlation are evaluated at the fluid saturation temperature [2].

that sprays could be characterized by the values of the spray hydrodynamic parameters measured at the geometric center. They incorrectly used a single boiling curve to determine the boundary heat flux at all surface locations being sprayed. They also presented results where a complex shape was uniformly sprayed at all surface locations, which is impossible to accomplish in a practical situation. Furthermore, Kim *et al.* and Wang *et al.* presented no experimental validation of their numerical models. Consequently, their results offer insight into neither the simulation nor the optimization of a spray quenching process.

Klinzing *et al.* [5] used the spray quenching heat transfer correlations [2, 5] and the spatial distribution models of the spray hydrodynamic parameters developed by Deiters and Mudawar [3] to simulate the spray quenching of a thin, stationary rectangular Al 1100 plate using the commercial finite element software package ANSYS. Near-surface temperature measurements corresponding to the center and outer edge of the spray field were in fair agreement with the numerical predictions. Rozzi *et al.* [9] attempted to simulate the spray quenching of a stationary Al 1100 L-shaped testpiece using ANSYS. They determined that section thickness and spray configuration have a significant effect on the cooling rate and cooling uniformity of the testpiece. The spatial distribution of the volumetric spray flux in the axial direction caused the problem to become highly three-dimensional. Consequently, their two-dimensional finite element model significantly overpredicted the heat transfer rate, and comparisons with experimental temperature measurements were inconclusive [10]. Mudawar and Deiters [3, 4] accurately predicted the temperature history of an Al 1100 block which was sprayed over one surface and whose other surfaces were well insulated. However, film boiling correlations were unavailable and, hence, they were able only to predict temperature response in the relatively low temperature boiling regimes (below about 200°C).

Other researchers have used the nonlinear inverse heat conduction method [11] to obtain the thermal boundary condition required by a numerical analysis. This method extrapolates the surface temperature–time history from thermocouples embedded near the surface of the quenched part. Zabaras *et al.* [12] quenched a stationary, cylindrical extrusion (93.4% aluminum, 4.6% magnesium) in an agitated water bath. The boundary condition for an axisymmetric finite element analysis, which predicted the temperature–time history and residual stress distribution within the part, was the surface temperature–time history determined using measured temperatures and the inverse heat conduction method. Good agreement

between measured and predicted temperatures was obtained at internal locations; thus, the prediction of residual stress was not hindered by an inaccurate thermal history. Once a material constitutive model, such as that proposed by Zabaras *et al.*, is experimentally validated, then it will become possible to accurately predict the residual stress distribution in complex-shaped parts using the methodology developed in the present study which, unlike [12], uses heat transfer correlations independent of part geometry to obtain the thermal boundary condition.

This review of previous research presented several key ideas as being crucial to the development of the CAD based intelligent spray quenching system. The present study examines the following aspects of this ongoing, cross-disciplinary research:

1. Can the spatial distribution models of the spray hydrodynamic parameters, developed by Mudawar and Deiters [3, 4], be simplified so that a single model adequately represents all nozzles of a given type?
2. Uniform cooling of a typical aluminum part requires multiple sprays impinging multiple surfaces. Thus, unlike previous studies [3, 4], the spray quenching experiments and models must simulate a realistic, industrial-like environment.
3. The final mechanical properties of heat treated aluminum alloys are critically dependent on the cooling history within a range of temperatures (320–420°C for Al 2024) which are associated with the film boiling regime for many types of sprays [13]. Thus, although the temperature response of parts to spray quenching below the film boiling regime has been successfully predicted [3, 4], the current investigation can not dismiss the existence of film boiling during the initial cooling of the part.
4. An array of overlapping sprays quenching a long part may cause large axial changes in the heat transfer coefficient; thus, invalidating two-dimensional numerical models [9, 10]. Can axial changes be effectively eliminated by optimizing nozzle spacing?

EXPERIMENTAL METHODS

Spray Characterization Facility

The Spray Characterization Facility shown in Fig. 2(a) was used to measure the volumetric spray flux distribution of the spray nozzles used in the present study. The facility has a 0.11 m^3 (30 gallon) reservoir within the spray chamber which is constructed from phenolic and painted internally with water resistant enamel. The spray chamber was partially fabricated from optical grade Lexan sheet to permit observation of the experiment. Three optical translation rails and a rack, pinion and rod assembly facilitated nozzle positioning to within 1 mm in the x, y and z directions. The fluid delivery loop consisted of stainless steel tubing and contained a stainless steel rotary vane pump, rated to deliver 2.8×10^{-4} m^3 s^{-1} (4.45 gpm) at 690 kPa (100 psi), and a 10 μm filter to ensure fluid purity. The relatively low flow rate required by a single nozzle necessitated the use of a bypass line back into the reservoir. A rotameter was used to measure the nozzle flow rate with a full-scale accuracy of $\pm 2\%$. Operating pressure was measured using a liquid filled stainless steel pressure gage with a range of 0–690 kPa (0–100 psi) and an accuracy of ± 6.9 kPa (1 psi).

A spray collector was mounted at the geometric center of the spray chamber and the translation stages were used to position the nozzle at any x–y–z location relative to the collector opening. Volumetric spray flux, Q'', was measured by collecting water in a 200 ml graduated cylinder with an inlet diameter of 1.0 cm and dividing the volume of water collected by the product of fill time and inlet area. The cylinder inlet was raised above the holding platform and sharpened to reduce any edge effects. Fluid exiting the nozzle impinged upon the spray collector and was either collected or drained into the bottom of the spray chamber for recirculation.

Particle sizing facility

A Phase Doppler Particle Analyzer (PDPA) manufactured by Aerometrics, Inc. was used to simultaneously measure drop size and drop velocity at discrete locations within the spray field. Several locations within the spray field were targeted in order to ascertain the spatial distribution of these parameters. Multiple tests were conducted at each location to ensure repeatability. The phase Doppler method requires no calibration because drop size and velocity depend only on laser wavelength and optical configuration. Measurements are not based upon scattered light intensity and, consequently, are not subject to errors from beam attenuation or deflection which occur in dense spray environments. The principles of light scattering interferometry and the physical limitations of the PDPA are discussed in detail by Bachalo and Houser [14].

Materials Processing Test Bed

The Materials Processing Test Bed, a cross-disciplinary initiative encompassing efforts from various engineering departments and located at the Purdue University Boiling and Two-Phase Flow Laboratory, was used to simulate the heat treatment process (solution heat treating, spray quenching, and artificial aging) of aluminum alloys in an industrial environment. Figure 2(b) shows a cut-away view of the test chamber of the Materials Processing Test Bed and a detailed schematic of the furnace and translation system. A Lindberg model 54857-V tube furnace, which has a cylindrical heating length of 60 cm and diameter of 15 cm, was utilized to heat the aluminum testpiece. The three independent heating zones of the furnace were regulated using a programmable controller, thus ensuring uniform heating of the testpiece. The process tube mounted inside the furnace protected the heating elements during testing. The testpiece rested on a pedestal with three posts that were bolted to the

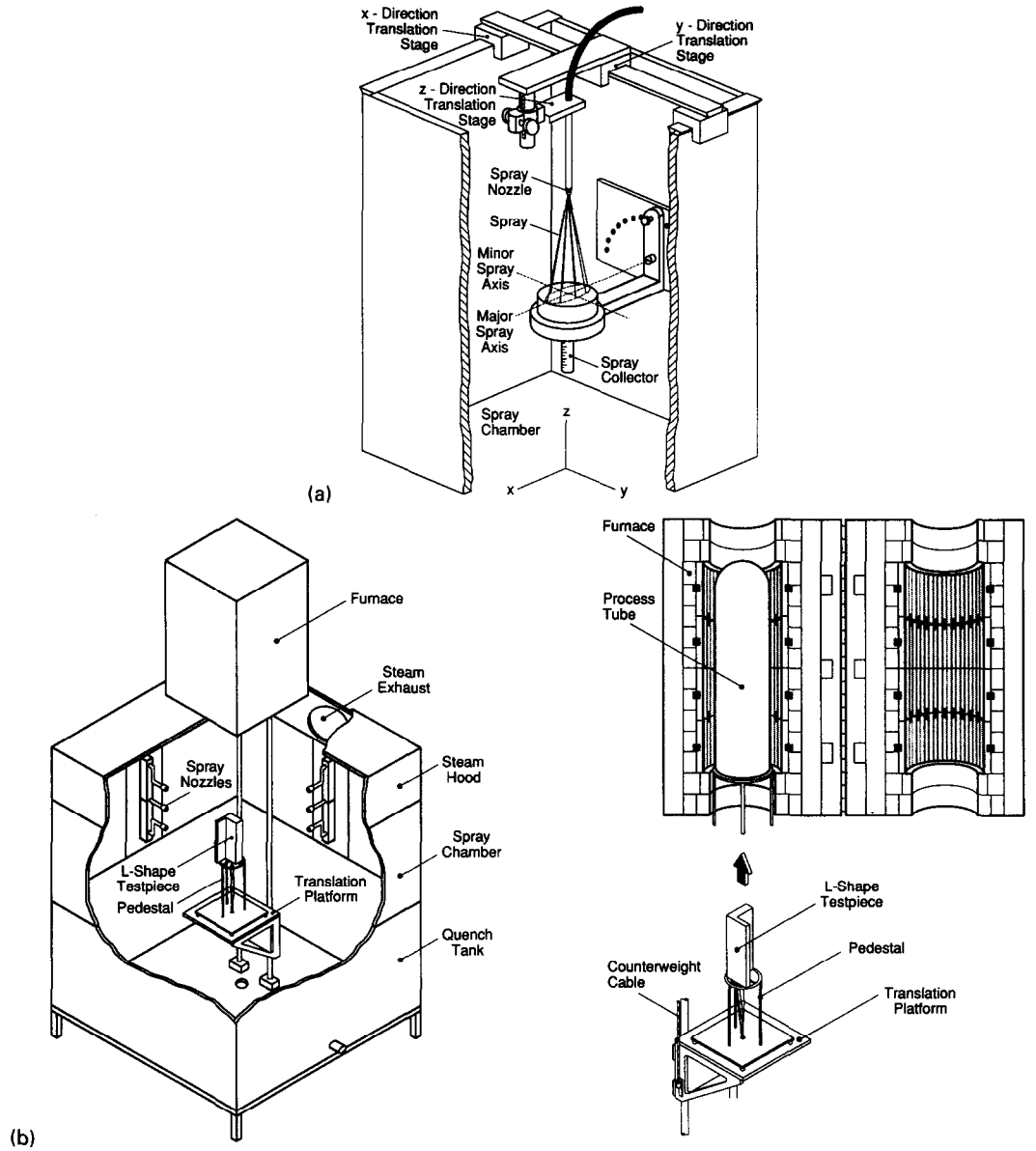

Fig. 2. (a) Cut-away view of the Spray Characterization Facility. (b) Cut-away view of the test chamber of the Materials Processing Test Bed and schematic of the furnace and testpiece translation system.

translation platform. The testpiece was lowered from the furnace into the spray chamber using a stainless steel cable connected to the back of the platform. The spray chamber was fabricated from optical grade Lexan sheet to permit observation of the spray quenching process. An exhaust system connected to the back of the test chamber removed steam produced by the quench. Water stored in the quench tank was circulated using a fan cooled centrifugal pump, rated to deliver 25.2×10^{-3} m^3 s^{-1} (40 gpm) at 690 kPa (100 psi). The large capacity of the pump required a bypass line back into the quench tank to maintain flow stability.

Four nozzle arrays, one on each side of the spray chamber, allowed some flexibility of nozzle positioning relative to the testpiece. Each nozzle array, which consisted of three nozzles vertically separated by 11.4 cm (4.5 in.), was independently controlled using a globe valve connected to a steel-reinforced flexible rubber hose. Glycerin filled stainless steel pressure gages, each having a range of 0–1.10 MPa (0–160 psi), were utilized to monitor nozzle pressure. The flat spray nozzles used in the present study were operated at a pressure of 552 kPa (80 psig) and a distance of 0.305 m (12 in.) from the testpiece.

Testing commenced with the raising of the testpiece into the furnace using the vertical translation system. Once the testpiece attained the solution heat treatment temperature (495°C for Al 2024), the pump was engaged and the sprays were allowed to reach hydrodynamic equilibrium. The testpiece was quickly lowered into the spray chamber using the translation

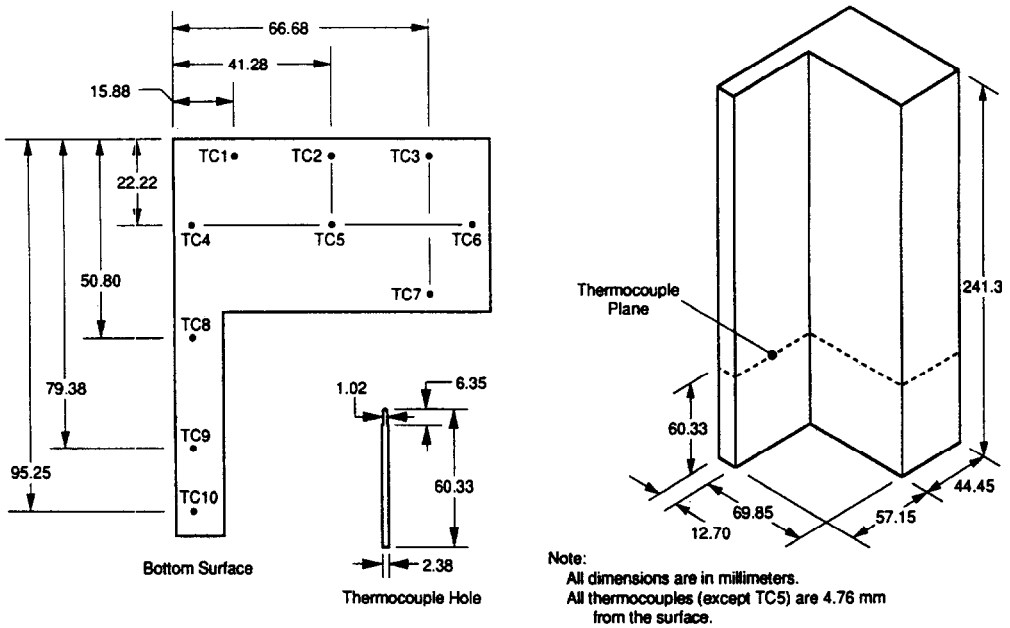

Fig. 3. Al 2024 L-shape dimensions and thermocouple placement.

system and thermocouple temperatures were recorded every 0.1 s throughout the quench.

L-shape testpiece

The L-shape testpiece shown in Fig. 3 was machined from an Al 2024 extrusion obtained from the Aluminum Company of America (ALCOA). The testpiece was designed so that the effects of section thickness on cooling uniformity could be investigated. The thick and thin protruding sections had a thermal mass ratio of 5:1. Ten Chromel–Alumel (type K) thermocouples, which consisted of 0.13 mm (0.005 in.) wire within a 0.81 mm (0.032 in.) diameter Inconel 600 sheathing with magnesium oxide insulation, were placed at strategic locations within the L-shape. The void surrounding the thermocouple bead was filled with boron nitride powder, which has a thermal conductivity comparable to aluminum; thus, excellent thermal contact with the aluminum was insured. The high temperature capabilities and adequate transient response of the type K thermocouple made it an excellent choice for the current application. All thermocouples were placed in a plane one-fourth the length of the L-shape above the lower surface. The testpiece surface was carefully polished to ensure uniform surface texture and repeatability between quenches. This procedure was required because surface roughness has been observed to effect the thermal response of spray quenched parts [10]. Furthermore, the spray quenching heat transfer correlations used in the present numerical study were obtained using polished surfaces [2, 5].

NUMERICAL METHODS

The numerical analysis of the spray quenching process involved solving the transient heat diffusion equation with temperature dependent material properties [15] and temperature and spatially dependent boundary conditions. The ability of the commercial finite element program ABAQUS [16] to solve this problem with a user defined nonuniform heat transfer coefficient made it ideal for the present study. Additional benefits included an efficient nonlinear equation solver and self-adaptive time stepping scheme.

Since the ultimate objective of the present research is to numerically optimize the quenching process by changing nozzle configurations, surfaces of the part may or may not be in contact with a water spray. The ABAQUS input file [17] was generalized to permit a convection boundary condition for all surface elements. Furthermore, the locations of large spatial temperature gradients were unknown; hence, a uniform finite element mesh was used. The input file contained a FORTRAN subroutine which defined the heat transfer coefficient as a function of surface temperature and surface location relative to the spray nozzles. The subroutine was consulted for each surface node at every iteration of every time increment. The subroutine performed the following tasks if the location was being sprayed: (1) local spray hydrodynamic parameters were determined, (2) boiling regime experienced at this location and (3) corresponding local surface heat flux were calculated using the spray quenching heat transfer correlations, and (4) convection heat transfer coefficient was defined as $h = q''/\Delta T$. Radiation heat transfer from sprayed surfaces was neglected since the heat transfer coefficient due to radiation alone (based on a surface temperature of 495°C and an emissivity of 0.15 [18]) was less than 0.6% of the lowest value of the heat transfer coefficient due to spray convection (deter-

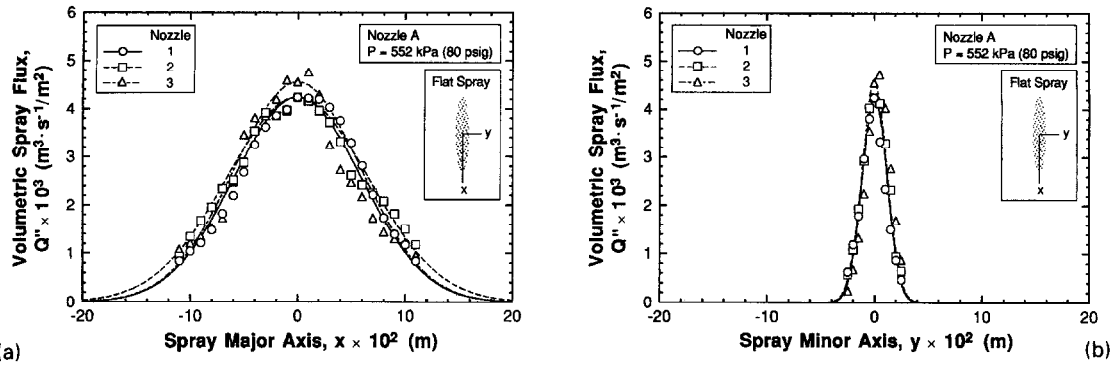

Fig. 4. Verification of the volumetric spray flux measurement technique on the (a) major axis and (b) minor axis of different type A nozzles.

mined using the film boiling correlation listed in Table 1 for a location near the edge of the spray field). Natural convection and radiation from unsprayed surfaces was found to have a negligible effect on the numerical results. The finite element program iterated each time increment until the solution at each node differed by less than 0.01°C between iterations. A nearly continuous temperature–time history was obtained by defining a maximum allowable time increment of 0.1 s. Solution convergence was investigated to determine the appropriate element type and size required by the present problem (1.25×1.25 mm^2 quadratic elements).

SPRAY INTERACTION

Single spray parameters

Visual examination of a typical flat spray nozzle revealed an elliptical spray pattern which was fairly symmetrical about the nozzle centerline. Mudawar and Deiters [3, 4] indicated that minute machining flaws caused the spray hydrodynamic parameters to have an asymmetric spatial distribution. They concluded that the parameters could be predicted for each nozzle using a unique asymmetric exponential function. However, an objective of the present study was to develop simple models which could be used with all nozzles of a given type without sacrificing accuracy. As indicated below, the same simple model used to describe spray pattern can also be used as a criterion for discarding flawed nozzles.

The volumetric spray flux, Q'', was defined as the local volume flow rate per unit surface area. The measurements shown in Fig. 4 revealed that the volumetric spray flux exhibits a maximum value near the center of the spray and decays exponentially along the major (x-axis) and minor (y-axis) axes of the elliptical pattern. Thus, the spatial distribution of the volumetric spray flux was modeled by the function

$$Q'' = A_0 \exp(A_1 x^2 + A_2 y^2) \quad (1)$$

where A_0 is the volumetric spray flux measured at the nozzle centerline and A_1 and A_2 are constants determined using the least squares curve fitting procedure. Off-axis measurements confirmed the predictive ability of equation (1) for all locations within the spray field at a given distance from the nozzle. The close agreement between curve fits shown in Fig. 4 demonstrate that the model developed using a single nozzle is applicable to all nozzles of that type. These same curve fits are also instrumental at ascertaining which nozzles of a given type should be discarded; those nozzles typically display skewed patterns which can be readily detected by comparison with the patterns of other nozzles of the same type.

The spray quenching heat transfer correlations used in the present study contain mean drop diameters and mean drop velocities instead of the complete drop size and drop velocity distribution of the spray. Sauter mean diameter, SMD or d_{32}, is the diameter of the drop whose ratio of volume to surface area is the same as that of the entire measurement sample. The mean drop velocity, U_m, is simply the average of measured individual drop velocities. d_{32} and U_m did not appear to vary considerably, or predictably, between measurement locations. Hence, the spray field at a distance of 0.305 m (12 in.) from the nozzle orifice was characterized by an average d_{32} and an average U_m. Table 2(a) summarizes the spatial distribution models of the spray hydrodynamic parameters for the flat spray nozzles used in the present study.

Hydrodynamic parameters of overlapping sprays

Typically, a quenching operation consists of either stationary parts or long extrusions moving through an array of spray nozzles. Relatively even spray coverage can be obtained when several nozzles with overlapping spray patterns are utilized. However, the nozzle spacing must be optimized to eliminate undesired axial changes in the heat transfer coefficient. Volumetric spray flux appears to be the primary spray hydrodynamic parameter controlling the spatial variation of the heat transfer rate since d_{32} and U_m are somewhat insensitive to location. The spray interaction between two adjacent nozzles was investigated and a methodology was developed for adapting the single nozzle models for use with nozzle arrays having overlapping spray patterns.

Table 2. (a) Spatial distribution models of the spray hydrodynamic parameters for the flat spray nozzles and (b) nozzle spacing required to achieve a one-dimensional volumetric spray flux distribution

(a)

Nozzle type	Pressure [kPa] ([psig])	Distance [m] ([in.])	Flow rate [$m^3 s^{-1} \times 10^6$] ([gpm])	$d_{32} \times 10^6$ [m]	U_m [$m s^{-1}$]	$Q''(x, y)$† [$m^3 s^{-1} m^{-2}$]
A	550 (80)	0.305 (12.0)	18 (0.28)	286	13.5	$Q'' = 4.24 \times 10^{-3} \exp(-143\,x^2 - 3790\,y^2)$
B	550 (80)	0.305 (12.0)	36 (0.57)	320	15.8	$Q'' = 9.91 \times 10^{-3} \exp(-134\,x^2 - 5470\,y^2)$

† The coordinates, x and y, shown in the $Q''(x, y)$ equations have units of meters.

(b)

Nozzle type	Optimum nozzle spacing [m] ([in.])	Mean spray flux† $\bar{Q}'' \times 10^3$ [$m^3 s^{-1} m^{-2}$]	Standard deviation† σ [$m^3 s^{-1} m^{-2}$]	Actual nozzle spacing‡ [m] ([in.])	Mean spray flux§ $\bar{Q}'' \times 10^3$ [$m^3 s^{-1} m^{-2}$]	Standard deviation§ σ [$m^3 s^{-1} m^{-2}$]
A	0.128 (5.04)	4.77	0.0377	0.114 (4.5)	5.32	0.197
B	0.132 (5.2)	11.1	0.0880	0.114 (4.5)	12.8	0.532

† These statistical parameters refer to the behavior of the theoretical volumetric spray flux at locations on the major axis between two nozzles separated by the optimum distance for that particular nozzle type. This data also assumes that the volumetric spray flux from each nozzle is additive at every location within the spray field.

‡ Nozzles are located at 0.006 m (0.25 in.), 0.121 m (4.75 in.) and 0.235 m (9.25 in.) along the L-shape testpiece which has a length of 0.241 m (9.5 in.).

§ These statistical parameters refer to the behavior of the theoretical volumetric spray flux at locations on the major axis along the L-shape testpiece. This data also assumes that the volumetric spray flux from each nozzle is additive at every location within the spray field.

The spatial distribution model of the volumetric spray flux was used to optimize nozzle spacing by assuming that the volumetric spray flux contributed by two adjacent nozzles was additive at all (x, y) locations and, thus, could be predicted by

$$Q'' = A_0 \exp[A_1(x-x_1)^2 + A_2(y-y_1)^2] + A_0 \exp[A_1(x-x_2)^2 + A_2(y-y_2)^2] \quad (2)$$

where (x_1, y_1) and (x_2, y_2) are the locations of the nozzle centerlines. This assumption was verified by modifying the fluid delivery loop of the Spray Characterization Facility to allow the simultaneous operation of two spray nozzles. Two type A nozzles (see Table 2(a) for nozzle designation) were aligned such that their major axes coincided. The nozzle spacing and nozzle-to-surface distance were identical to those used in the Materials Processing Test Bed. As shown in Fig. 5(a), the combined volumetric spray flux from simultaneous operation of both nozzles compared well with the values obtained using the superposition of two single nozzle models; thus, confirming the additivity of volumetric spray flux.

The following procedure was used to optimize nozzle spacing: (1) The distribution of volumetric spray flux along the major axis between two adjacent nozzles was predicted using equation (2), (2) the corresponding standard deviation of the volumetric spray flux along the major axis was calculated and (3) the optimum nozzle spacing was determined by changing the nozzle spacing until a minimum standard deviation was obtained. Table 2(b) presents the optimum nozzle spacing and corresponding statistical parameters for the nozzles used in the present study. $\bar{Q}''$ represents the mean volumetric spray flux along the major axis of the spray field. Figures 5(b1)–5(b3) compare the two-dimensional volumetric spray flux distribution for two type A nozzles separated by the optimum distance, a smaller distance, and a larger distance. As the difference between the actual nozzle spacing and the optimum nozzle spacing increases, the distribution of the volumetric spray flux between the two nozzles becomes less uniform. This condition will produce undesirable axial nonuniformity in the heat transfer coefficient along the surfaces of long extrusions.

The two-dimensional finite element analysis of the quenching process requires knowledge of the volumetric spray flux distribution for a plane parallel to the spray minor axis. The presence of multiple, partially overlapping sprays causes the distribution on the minor axis to deviate from the single nozzle model. If the nozzle spacing is near the optimum value, then the distribution along all planes parallel to the spray

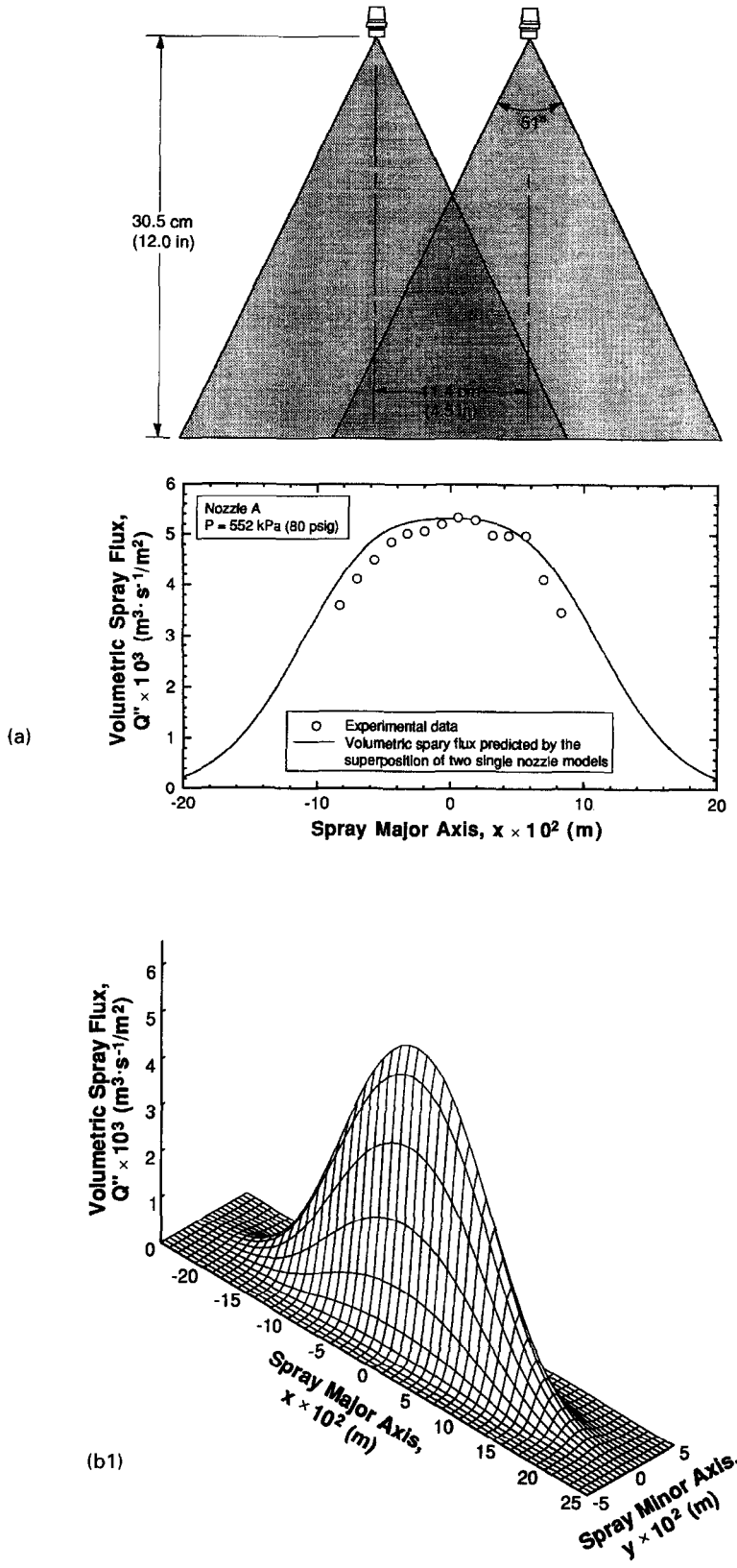

Fig. 5. (a) Volumetric spray flux distribution on the major axis of two type A nozzles separated by 11.4 cm (4.5 in.), and spatial distribution model of the volumetric spray flux for two type A nozzles separated by (b1) 8.9 cm (3.5 in.), (b2) 12.8 cm (5.04 in.) and (b3) 16.5 cm (6.5 in.).

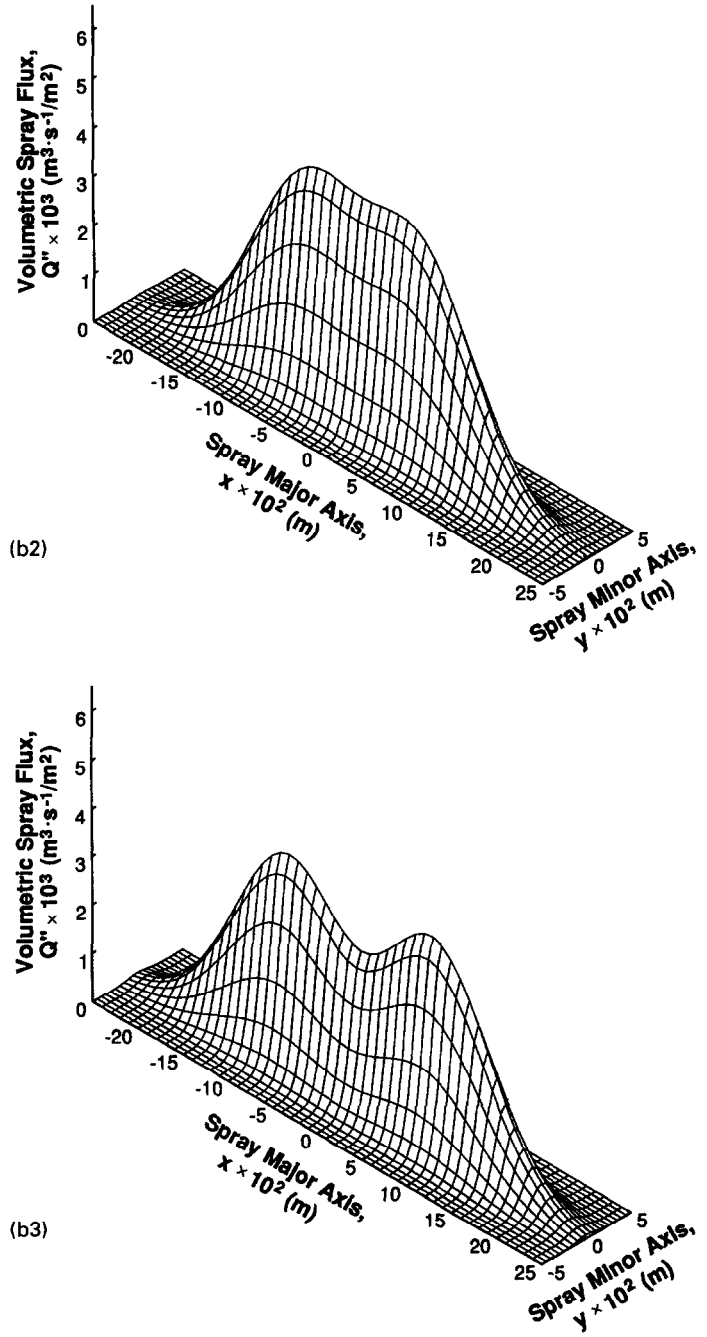

Fig. 5—*continued.*

minor axis will be fairly identical. It is proposed that the coefficient A_0 in equation (1) can be replaced with the mean value of the volumetric spray flux along the major axis of the nozzle configuration, $\bar{Q}''$, without sacrificing accuracy. Thus, the volumetric spray flux distribution for a plane parallel to the spray minor axis becomes

$$Q'' = \bar{Q}'' \exp(A_2 y^2). \quad (3)$$

This assumption is justified if the standard deviation of the volumetric spray flux along the major axis is a small percentage (about 5%) of $\bar{Q}''$.

The nonoptimized nozzle configuration used in past studies [5, 9, 10] consisted of two flat spray nozzles (different from those used in the present study) separated by 12.1 cm (4.75 in.) and had $\sigma/\bar{Q}'' = 0.19$. This nozzle configuration produced significant axial temperature gradients in the stationary testpiece and, hence, the testpiece could not be analyzed using a two-dimensional numerical model. The nozzle con-

figuration used in the present study (see Table 2(b)) consisted of three nozzles separated by 11.4 cm (4.5 in.) and had $\sigma/\bar{Q}'' = 0.037$ and 0.042 for nozzle types A and B, respectively. The nozzle configuration used in the present study satisfies $\sigma/\bar{Q}'' < 0.05$; thus, eliminating the majority of the axial temperature gradients and permitting the quenching process to be analyzed using a two-dimensional numerical model.

Negligible droplet interactions, such as drop coalescence or deflection, between adjacent sprays was an inherent assumption of volumetric spray flux additivity. An exception to this rule is an extremely dense spray which will have an optimal nozzle spacing larger than predicted due to droplet interactions between sprays. This assumption also permits a nozzle array containing one nozzle type to be characterized by a single value of the Sauter mean diameter and mean drop velocity. Hence, the values of these parameters shown in Table 2(a) can be applied without modification to any nozzle configuration. Since the spray hydrodynamic parameters can be determined at any location within the spray using the previously discussed models, it is possible to utilize these models with the spray quenching heat transfer correlations to predict the spatial distribution of the heat transfer coefficient.

It is quite impractical and cost prohibitive to measure the distribution of the spray hydrodynamic parameters of all nozzles used in a heat treatment operation. Consequently, the models developed using a few nozzles must be applicable to all nozzles of that type. Therefore, based on experience with the present system, the following guidelines should be observed to insure reliable and predictable nozzle performance:

1. Stainless steel nozzles, or nozzles made from another corrosion and erosion resistant material, should be used since a harsh environment will cause inexpensive (e.g. brass) nozzles to corrode, thus altering the nozzles performance.
2. All nozzles should be tested periodically. The flow rate and spray angle of the nozzles should be measured and compared to the manufacturer's specifications.
3. The spray pattern should be visually examined when installed and periodically during use. Nozzles with irregularities (unsymmetrical spray pattern, deflected spray, damaged orifice) should be discarded.
4. When nozzles are mounted in tees, manifolds or elbows, jet stabilizers should be used to reduce internal flow turbulence which could lead to a distorted spray pattern.
5. The fluid delivery loop should contain a filter capable of removing particles which could obstruct the nozzle orifice and, as a backup, a removable nozzle strainer should be placed immediately before the nozzle orifice.

NUMERICAL SIMULATION OF THE QUENCHING PROCESS

Spray quenching tests were conducted using the Materials Processing Test Bed in order to experimentally investigate the ability of the approach developed in the present study to predict the cooling history of the Al 2024 L-shape testpiece. The results presented in this study assumed that heat transfer was two-dimensional, which was an acceptable assumption for nozzles A and B and the current nozzle spacing in the Materials Processing Test Bed. The temperature predicted by the two-dimensional finite element analysis was compared with measured temperatures obtained from thermocouples located in a plane one-fourth of the entire testpiece length above the lower surface. Verification of these temperature predictions was necessary before mechanical properties could be predicted in a heat treated part.

Impact of transitions between boiling regimes

Figure 6 shows the predicted temperature distribution along the outer sprayed surfaces of the thick and thin sections for a quench using type A nozzles. The boiling regimes indicated in the figure correspond to surface conditions along the spray centerline (i.e. major axis of the spray field). During film boiling, the surfaces cool relatively uniformly. The upper left side of the L-shape cools the slowest since this side is unsprayed. The right edge of the thick section cools fairly quickly compared to locations near the center of the impinging spray since both the top and right surfaces of the thick section are being sprayed. Once the surfaces enter the transition boiling regime, the cooling rate increases substantially as evidenced by the large temperature drop and short time period between the point of minimum heat flux and the point of critical heat flux. The nucleate boiling regime is also short-lived since it is characterized by a small range of surface temperatures and enormous heat transfer coefficients. Finally, the majority of the sprayed surfaces enter the single-phase cooling regime while the unsprayed surface locations are still at high temperatures. This phenomenon causes the unsprayed surfaces to be cooled by conduction to areas which are being heavily sprayed.

Figures 7(a)–7(f) display isotherms of the L-shape at various times throughout a quench using type A nozzles. The isotherms are spaced 20°C apart and the maximum and minimum temperatures are also shown at each time. As expected, the thin section cools the quickest while the upper left side remains the hottest during all stages of the quench. At 5 s, all sprayed surfaces are undergoing film boiling and spatial temperature gradients are relatively small. Ten seconds later, the thin section begins to enter the transition boiling regime. At 20 s, the thin section has progressed into the single-phase cooling regime while the remaining surfaces are still experiencing film boiling. The enormous heat transfer rates present in the thin sec-

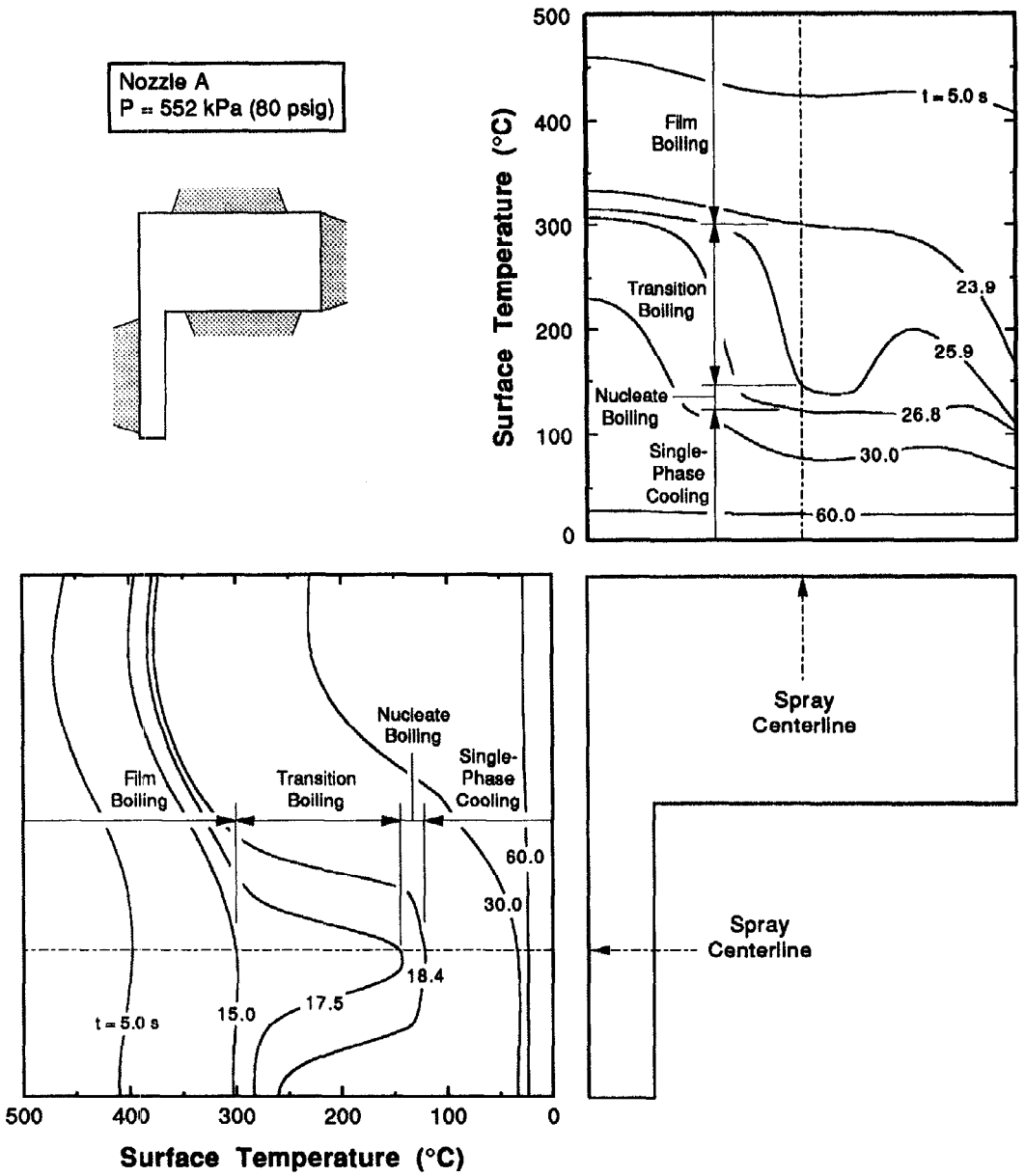

Fig. 6. Temperature distribution along sprayed surfaces of the L-shape for a quench using type A nozzles. The identified transitions between boiling regimes correspond to the spray centerline of the respective sprayed surface.

tion cause it to become a more favorable path for heat flow. Thus, the thick section becomes cooled by conduction to the thin section in addition to the sprayed surfaces of the thick section. The upper right corner of the thick section is well into nucleate boiling at 25 s and large temperature gradients are observed over a large portion of the cross-section. The other surfaces of the thick section are experiencing a range of boiling regimes: film boiling near the upper left side to nucleate boiling at the upper right corner. At 30 s, the entire L-shape is well below the critical temperature range (320–420°C for Al 2024) and, hence, the mechanical properties have been determined. Thirty-five seconds after initiating the quench, boiling has completely subsided on all surfaces and heat transfer is simply the result of single-phase forced convection to the water sprays.

The isotherms presented in Figs. 7(a)–7(f) are an invaluable tool for determining areas of high and low temperature gradients within the part. Overall, large temperature gradients occur immediately after the surface begins experiencing transition boiling and persist until all sprayed surfaces enter the single-phase cooling regime. The closely spaced isotherms at 20

and 25 s show large temperature gradients exist within the part, even at locations away from the sprayed surfaces. The upper left side of the L-shape experiences relatively low temperature gradients throughout the quench due to the absence of a spray in this area. Note that, in all cases, the isotherms along the unsprayed upper left side are perpendicular to the surface; thus, confirming heat transfer due to radiation and free convection is negligible compared to convection from a sprayed surface. Future experimental studies will use this type of numerical information to reduce spatial temperature gradients within the part by modifying the nozzle configuration; thus, reducing residual stresses in the heat treated part.

Validation of numerical predictions

Figure 8(a) compares the finite element temperature predictions with the measured temperature–time curves of the L-shape for a quench using type A nozzles. Two experimental temperature–time curves are shown for each thermocouple to demonstrate that the spray quenching experiments are repeatable. TC 4, which is near an unsprayed surface, and TC 5, which is in the center of the thick section, cool at approximately the same rate. TC 7, which is near two sprayed surfaces, cools quicker, both experimentally and numerically, than TC 5. The lower graph in Fig. 8(a) compares TC 9, which is the fastest cooling thermocouple, to TC 5. The finite element tem-

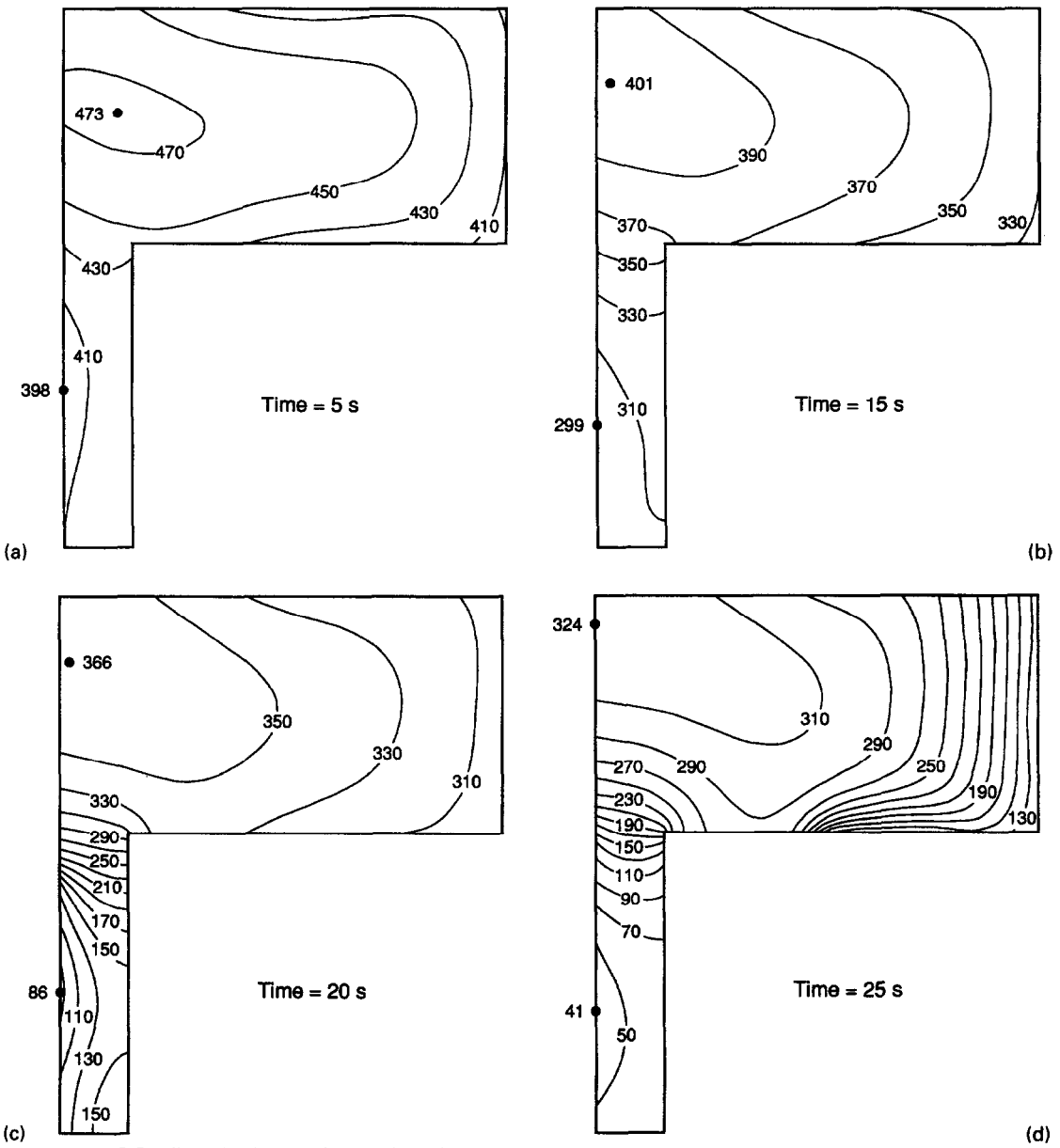

Fig. 7. Predicted isotherms of the L-shape for a quench using type A nozzles at (a) 5, (b) 15, (c) 20, (d) 25, (e) 30 and (f) 35 s.

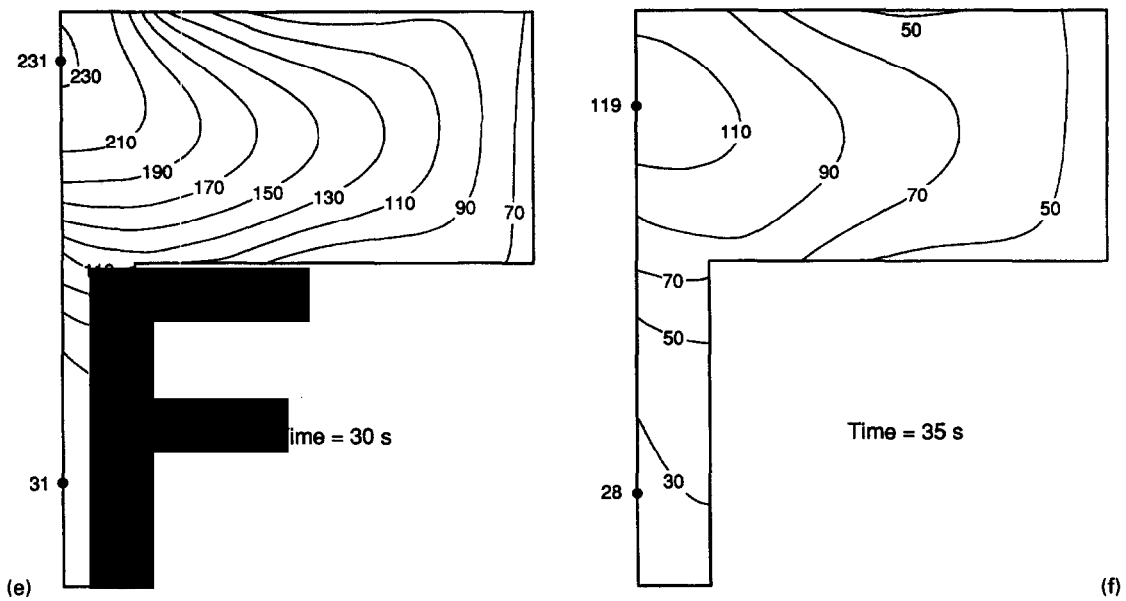

Fig. 7—*continued.*

perature predictions for the four thermocouples compare quite well with experiment. Minor discrepancies are observed near the temperature at the point of minimum heat flux for those thermocouples adjacent to sprayed surfaces, TC 7 and TC 9. The temperature–time curves of thermocouples not presented in Fig. 8(a) are in similar agreement with the finite element predictions. Figure 8(b) shows the temperature comparisons for a quench using type B nozzles whose volumetric spray flux is more than twice that of type A nozzles. The predictions are good considering that the spray flux correlations are being applied to surfaces having a slightly larger volumetric spray flux than specified by Klinzing *et al.* [5]. TC 7 disagrees

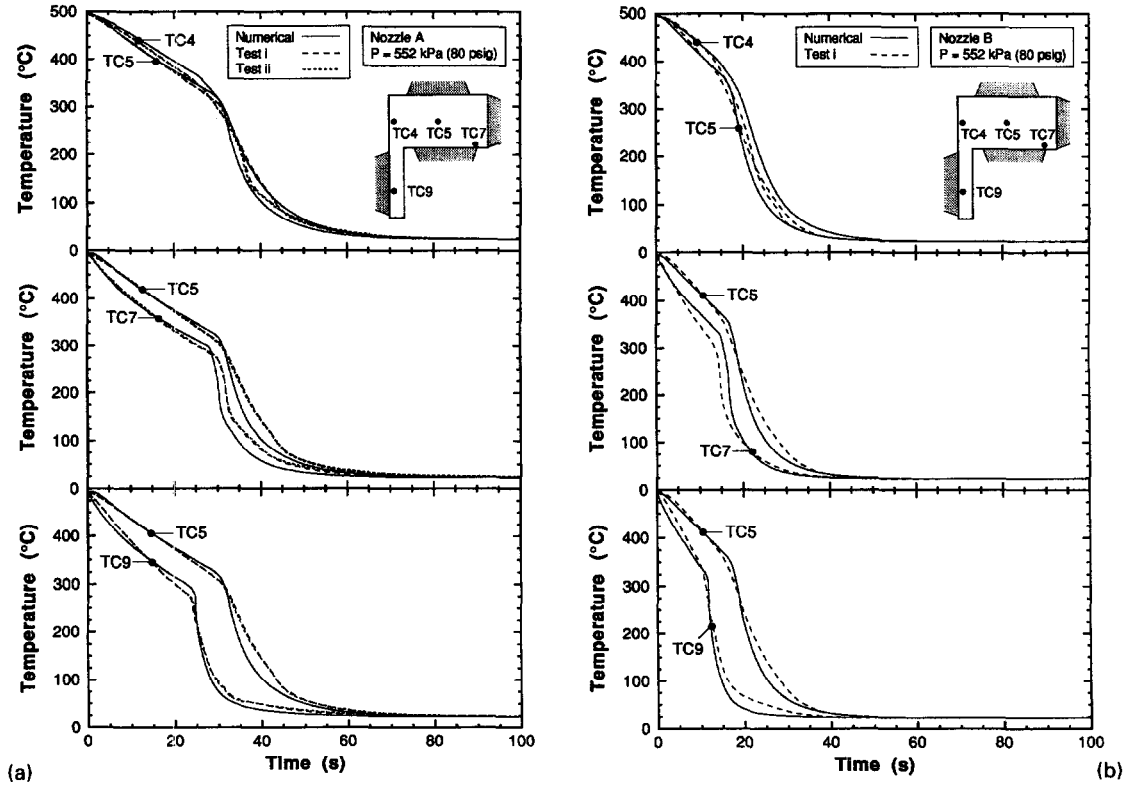

Fig. 8. Comparison of the finite element temperature predictions with measured temperature–time curves of the L-shape for a quench using type (a) A and (b) B nozzles.

the most with the experiment, probably because it is near two sprayed surfaces. Figures 8(a) and 8(b) confirm that the method developed in the present study accurately predicts the thermal history of metallic parts subjected to spray quenching.

CONCLUSIONS

This study continues the development of the CAD based intelligent spray quenching system, originally proposed by Deiters and Mudawar [1], which, once completed, will optimize the quenching of aluminum alloys to achieve superior part quality. The primary goal of the present study was to develop a method for predicting the temperature–time history of complex-shaped aluminum alloy parts subjected to spray quenching. Key conclusions from this study are as follows:

1. The spatial distribution of the spray hydrodynamic parameters was investigated for two nozzle types. The volumetric spray flux distribution was well represented by a curve-fit which exhibited a maximum value near the center of the spray and decayed exponentially away from the center. The mean drop diameter and mean drop velocity did not vary significantly within the spray field; hence, average values were determined for each nozzle.

2. Spray interaction between adjacent nozzles whose major axes coincide was investigated and the nozzle separation distance along the major axis of the spray field was optimized. A methodology was developed for adapting the single nozzle models for use with nozzle arrays having overlapping spray patterns.

3. The temperature–time history of a complex-shaped part quenched with multiple, partially overlapping spray nozzles was successfully predicted using the methodology developed in the current study and the spray quenching heat transfer correlations developed by Mudawar and Valentine [2] and Klinzing *et al.* [5].

4. The coupling of the microstructure evolution with the predicted temperature–time history [13] should enable the determination of the final mechanical properties *a priori*; hence, the performance of a spray quenching system can be judged prior to operation. Once perfected, the CAD based intelligent spray quenching system will significantly reduce cost and increase productivity.

Acknowledgements—The authors gratefully acknowledge the financial support of the Purdue University Engineering Research Center for Intelligent Manufacturing Systems. Financial support for the first author was provided in the form of the United States Department of Energy Predoctoral Integrated Manufacturing Fellowship. The authors also thank Jerry Hagers, Rudolf Schick and Chris Schaffer of Spraying Systems Company for their valuable technical assistance.

REFERENCES

1. T. A. Deiters and I. Mudawar, Optimization of spray quenching for aluminum extrusion, forging, or continuous casting, *J. Heat Treat.* **7,** 9–18 (1989).
2. I. Mudawar and W. S. Valentine, Determination of the local quench curve for spray-cooled metallic surfaces, *J. Heat Treat.* **7,** 107–121 (1989).
3. T. A. Deiters and I. Mudawar, Prediction of the temperature–time cooling curves for three-dimensional aluminum products during spray quenching, *J. Heat Treat.* **8,** 81–91 (1990).
4. I. Mudawar and T. A. Deiters, A universal approach to predicting temperature response of metallic parts to spray quenching, *Int. J. Heat Mass Transfer* **37,** 347–362 (1994).
5. W. P. Klinzing, J. C. Rozzi and I. Mudawar, Film and transition boiling correlations for quenching of hot surfaces with water sprays, *J. Heat Treat.* **9,** 91–103 (1992).
6. K. J. Choi and S. C. Yao, Mechanisms of film boiling heat transfer of normally impacting spray, *Int. J. Heat Mass Transfer* **30,** 311–318 (1987).
7. J. S. Kim, R. C. Hoff and D. R. Gaskell, A quench factor analysis of the influence of water spray quenching on the age-hardenability of aluminum alloys, *Proceedings of the International Symposium on Materials Processing in the Computer Age*, pp. 203–221. Minerals, Metals & Materials Society, New Orleans, LA (1991).
8. K. F. Wang, S. Chandrasekar and H. T. Y. Yang, An efficient 2D finite element procedure for the quenching analysis with phase change, *ASME J. Engng Ind.* **115,** 124–138 (1993).
9. J. C. Rozzi, W. P. Klinzing and I. Mudawar, Effects of spray configuration on the uniformity of cooling rate and hardness in the quenching of aluminum parts with nonuniform shapes, *J. Mater. Engng Perform.* **1,** 49–60 (1992).
10. J. C. Rozzi, Quenching of aluminum parts having irregular geometries using multiple water sprays, M.S. Thesis, Purdue University, West Lafayette, IN (1991).
11. J. V. Beck, Nonlinear estimation applied to the nonlinear inverse heat conduction problem, *Int. J. Heat Mass Transfer* **13,** 703–716 (1970).
12. N. Zabaras, S. Mukherjee and W. R. Arthur, A numerical and experimental study of quenching of circular cylinders, *J. Therm. Stresses* **10,** 177–191 (1987).
13. D. D. Hall and I. Mudawar, Predicting the impact of quenching on mechanical properties of complex-shaped aluminum alloy parts, *ASME J. Heat Transfer*, in press.
14. W. D. Bachalo and M. J. Houser, Phase/Doppler spray analyzer for simultaneous measurements of drop size and velocity distributions, *Opt. Engng* **23,** 583–590 (1984).
15. C. F. Lucks and H. W. Deem, *Thermal Properties of Thirteen Metals.* ASTM STP 227, p. 11 (1958).
16. Hibbitt, Karlsson and Sorensen, Inc., *ABAQUS User's Manual, Ver.* 4.8. Hibbitt, Karlsson and Sorensen Inc., Providence, RI (1989).
17. D. D. Hall, A method of predicting and optimizing the thermal history and resulting mechanical properties of aluminum alloy parts subjected to spray quenching, M.S. Thesis, Purdue University, West Lafayette, IN (1993).
18. G. G. Gubareff, J. E. Janssen and R. H. Torborg, *Thermal Radiation Properties Survey* (2nd Edn). Honeywell Research Center, Minneapolis, MN (1960).